Topological charge-density-vector method of identifying filaments of scroll waves

Yin-Jie He [1], Yuan-Xun Xia [1], Jin-Tao Mei [1], Kuangshi Zhou [2], Chenyang Jiang [2], Jun-Ting Pan [3], Dafang Zheng [1], Bo Zheng [4,1,*] and Hong Zhang [1,†]

[1] Zhejiang Institute of Modern Physics, School of Physics, Zhejiang University, Hangzhou 310058, China
[2] Department of Cardiology, Sir Run Run Shaw Hospital, School of Medicine, Zhejiang University, Hangzhou 310016, China
[3] Ocean College, Zhejiang University, Zhoushan 316021, China
[4] School of Physics and Astronomy, Yunnan University, Kunming 650091, China

(Received 3 May 2022; revised 21 August 2022; accepted 9 January 2023; published 30 January 2023)

Scroll waves have been found in a variety of three-dimensional excitable media, including physical, chemical, and biological origins. Scroll waves in cardiac tissue are of particular significance as they underlie ventricular fibrillation that can cause sudden death. The behavior of a scroll wave is characterized by a line of phase singularity at its organizing center, known as a filament. A thorough investigation into the filament dynamics is the key to further exploration of the general theory of scroll waves in excitable media and the mechanisms of ventricular fibrillation. In this paper, we propose a method to identify filaments of scroll waves in excitable media. From the definition of the topological charge of filaments, we obtain the discrete expression of the topological charge-density vector, which is useful in calculating the topological charge vectors at each grid in the space directly. The set of starting points of these topological charge vectors represents a set of phase singularities, thereby forming a line of phase singularity, that is, a filament of a scroll wave.

DOI: 10.1103/PhysRevE.107.014217

I. INTRODUCTION

Excitable media governed by reaction-diffusion equations support vortexlike rotating waves known as spiral waves in two dimensions, and scroll waves in three dimensions [1,2]. These vortices are involved in the spatiotemporal organization of wave dynamics in various complex systems of physical, chemical, and biological origins [3–5]. One of the most important examples is the onset of scroll waves in the heart, as they may cause the most dangerous cardiac arrhythmias [6–8]. Furthermore, three-dimensional rotors (scroll waves) are identified during sustained ventricular fibrillation, and it is shown that the presence of scroll waves and their dynamics determines the ventricular fibrillation duration [9].

Scroll waves in three dimensions are extensions of spiral waves in two dimensions [10–14]. A scroll wave is usually characterized by its filament [15], which is an extension into three dimensions of the tip (i.e., the phase singularity) of a spiral wave. The global behavior of a scroll wave is quite complex, but some features can be well described by the motion of its filament. Studies of the filament dynamics are important for the general theory of scroll waves in excitable media, as well as for applications in cardiac electrophysiology. Thus, the identification of filaments is particularly important.

For a stationary or slowly drifting scroll wave, a filament can be found by time-averaging sequential frames over one rotation cycle of the scroll wave [16,17]. The method is based on the established fact that the filament is surrounded by an area which is never excited by the circulating excitation wave. However, excitation patterns during ventricular fibrillation are not stationary and hence there is a need for algorithms that can identify filaments from short sections of data.

The filament can also be defined as the line where the excitation wavefront meets the repolarization wave back. The so-called zero-normal-velocity method [18] consists of finding the line on a chosen isopotential surface which exhibits a zero time derivative, i.e., finding the intersection of two successive isopotential surfaces. This method for the identification of filaments is independent of phase while the phase analysis of cardiac electrical signals sometimes is of great significance because it brings benefits to the study of the phase singularity of spiral waves [19,20].

Bray and Wikswo [21] developed the convolution method to identify the filament by using the concept of phase, which is a robust methodology to detect filaments. However, the convolution kernel of the convolution method has two different forms [22]. The final calculation results will also vary with the change of the convolution kernel. That is, one result is satisfied while the other is not well satisfied [23]. There is still a lack of appropriate theoretical explanations for this issue because the convolution method actually evolved from image processing techniques [21].

From the above discussions, developing a robust method to determine the filament with a strict theoretical derivation is still an academic topic of concern. In this paper, a method for the identification of filaments is proposed, named the topological charge-density-vector method. According to the concept of the topological charge and the topological current theory, we derive the theoretical expression of the topological charge-density vector in three-dimensional discrete space,

*Corresponding author: zhengbo@zju.edu.cn
†Corresponding author: hongzhang@zju.edu.cn

thereby obtaining the spatial distribution of topological charge vectors. Topological charge vectors distributed in the space carry a lot of information about the filament, such as the direction of the filament passing through a section, the location of the filament in the space, and so on. Among them, the filament localization is determined by the positions of starting points of topological charge vectors. Then we verify the practicability and stability of this proposed method in the FitzHugh-Nagumo (FHN) model. Here we use this method to detect filaments of different shapes, including linked and knotted filaments. In the Bär model, we test the performance of this method in detecting complex filaments of scroll wave turbulence. Finally, we apply this method to scroll wave turbulence in the Luo-Rudy model of cardiac tissue.

II. MODELS

In cardiac studies, the presence of scroll waves must be inferred from epicardial or endocardial recordings [24–26]. Thus numerical models of excitable media are valuable in providing information about the dynamic properties of filaments.

A. FitzHugh-Nagumo model

To illustrate our method, we first consider a classic two-variable FHN model [27,28] which is widely used as a mathematical model to describe an excitable medium. It is given by the following two-variable reaction-diffusion equations:

$$\frac{\partial V}{\partial t} = \frac{1}{\varepsilon}\left(V - \frac{V^3}{3} - W\right) + D\nabla^2 V, \tag{1a}$$

$$\frac{\partial W}{\partial t} = \varepsilon(V + \beta - \gamma W), \tag{1b}$$

where $V(\vec{r}, t)$ is the fast (voltage) variable while $W(\vec{r}, t)$ represents the recovery (gating) variable; D is the diffusion coefficient; ε, β, and γ are model parameters. In this paper, we set $D = 1.00$, $\varepsilon = 0.22$, $\beta = 0.70$, and $\gamma = 0.80$. The value V^* is set to be -1.139 [29]. We adopt an explicit Euler method to solve the FHN equations (1) in a spatial region which is a cube of $Lx = Ly = Lz = 100$, with a time step $\Delta t = 0.01$ and a space step $\Delta x = \Delta y = \Delta z = 0.5$. No-flux boundary conditions are employed on all boundaries of the medium. With these FHN model parameters, spiral waves are rotating in a two-dimensional medium with the period $T = 13.114$, which is a characteristic time for the excitable system.

B. Bär model

To figure out the performance of the topological charge-density-vector method in detecting complex and chaotic filaments, we use the Bär model [30] to exhibit scroll wave turbulence. Involving activator V and inhibitor W variables, this system can be described as

$$\frac{\partial V}{\partial t} = f(V, W) + D\nabla^2 V, \tag{2a}$$

$$\frac{\partial W}{\partial t} = g(V, W). \tag{2b}$$

Here $f(V, W) = \varepsilon^{-1} V(1-V)[V-(W+b)/a]$, and $g(V, W) = -W$ if $0 < V < \frac{1}{3}$; $g(V, W) = 1-6.75V(V-1)^2-W$ if $\frac{1}{3} \leqslant V \leqslant 1$; $g(V, W) = 1-W$ if $V > 1$ [30]. The diffusion coefficient D is set to be a unit and the parameters $a = 0.84$ and $b = 0.07$ are fixed to make sure that the system is excitable [30]. ε is the parameter controlling the intrinsic dynamics of scroll waves and $\varepsilon = 0.077$ is chosen to ensure the scroll waves will break up into turbulence. We set $V^* = 0.66$ for phase calculation. An explicit Euler method is adopted to solve Eq. (2) in a spatial region which is a cube of $Lx = Ly = Lz = 44$, with a time step $\Delta t = 0.01$ and a space step $\Delta x = \Delta y = \Delta z = 0.4$. No-flux boundary conditions are employed on all boundaries of the medium.

C. Luo-Rudy model

In order to make sure that the topological charge-density-vector method is available when applying to the study of the filament dynamics in cardiac modeling, we make a further investigation into its performance in the Luo-Rudy model [31]. The Luo-Rudy model is used as an action potential description of cardiac dynamics and it is given by

$$\frac{\partial V}{\partial t} = -\frac{I_{\text{ion}}}{C_m} + \nabla \cdot (D\nabla V), \tag{3}$$

where V is the transmembrane potential, C_m is the membrane capacitance, D is the diffusion constant, and I_{ion} is the total ionic current density of the membrane. All the parameters used in this paper are chosen to be the same as those in Fig. 3A(d) in Ref. [32], which will lead to the scroll wave turbulence. $V^* = -35.0$ mV is set for phase calculation. We use the Euler method to integrate Eq. (3) on a $4.4\,\text{cm} \times 4.4\,\text{cm} \times 1.8\,\text{cm}$ three-dimensional medium with a spatial step $\Delta x = \Delta y = \Delta z = 0.02$ cm and a time step $\Delta t = 0.01$ ms. No-flux boundary conditions are employed on all boundaries of the medium.

III. METHODS

A. Topological charge-density-vector method

Though a phase can be directly achieved from the two state variables in numerical simulations, there is only one observable variable (V, for instance) that may be recorded at a time for practical purposes. Experimentally, a reconstructed state space [19], generally formed by voltage $V(t)$ and $V(t + \tau)$, is used to calculate the phase with only one state variable. The pseudo-empirical mode decomposition (PEMD) [33,23] is an effective way to detrend the fast variable V, and after that the expression of the phase for each grid is

$$\phi(\vec{r}, t) = \arctan 2[V(\vec{r}, t + \tau) - V_{\text{mean}}(\vec{r}, t + \tau), V(\vec{r}, t) - V_{\text{mean}}(\vec{r}, t)], \tag{4}$$

where the function arctan 2 will return a value of the phase within $(-\pi, +\pi]$. However, using the PEMD to process the data is complex and time consuming in a three-dimensional case. For simplicity, we replace V_{mean} with the constant V^* as described in Ref. [19], i.e.,

$$\phi(\vec{r}, t) = \arctan 2[V(\vec{r}, t + \tau) - V^*, V(\vec{r}, t) - V^*]. \tag{5}$$

The time delay τ is taken to be $0.1T$.

Let there be a closed circuit Γ surrounding the filament, giving this circuit an arbitrary direction and starting from a point of origin on this circuit. If the phase ϕ turned in the hodograph is $\Delta\phi$, the topological charge n_t will be equal to $\Delta\phi/2\pi$, namely,

$$n_t = \frac{1}{2\pi}\oint_\Gamma \vec{K}\cdot d\vec{l}, \quad \vec{K} = \nabla\phi, \tag{6}$$

where $n_t = +1$ or $n_t = -1$. Using the Stokes theorem, we get

$$n_t = \frac{1}{2\pi}\iint_S (\nabla\times\vec{K})\cdot d\vec{\sigma}, \tag{7}$$

where the surface S is surrounded by Γ in Eq. (6). Thus, the charge-density vector is expressed as

$$\vec{\rho}(\vec{r}) = \frac{1}{2\pi}\nabla\times\vec{K}. \tag{8}$$

On the other hand, according to the topological current theory [34,35], the charge-density vector $\vec{\rho}(\vec{r})$ can be given by

$$\vec{\rho}(\vec{r}) = \delta[V(\vec{r},t+\tau)-V^*]\delta[V(\vec{r},t)-V^*]\vec{D}(V/x), \tag{9}$$

where δ is the Dirac's delta function; $\vec{D}(V/x)$ is the Jacobian determinant vector, whose components are

$$D^1(V/x) = \partial_y V(t)\partial_z V(t+\tau) - \partial_z V(t)\partial_y V(t+\tau),$$
$$D^2(V/x) = \partial_z V(t)\partial_x V(t+\tau) - \partial_x V(t)\partial_z V(t+\tau),$$
$$D^3(V/x) = \partial_x V(t)\partial_y V(t+\tau) - \partial_y V(t)\partial_x V(t+\tau).$$

As shown in Ref. [35], with the solution $\vec{r}_f(s)$ of the filament, we have

$$\vec{\rho}(\vec{r}) = n_t\int d\vec{r}_f\,\delta^3(\vec{r}-\vec{r}_f). \tag{10}$$

This means that $\vec{\rho}(\vec{r})$ is infinite at $\vec{r}_f(s)$ and zero at other positions.

After discretization, the topological charge-density vector $\vec{\rho}(\vec{r})$ can be written as a discrete expression, i.e.,

$$\vec{\rho}(i,j,k) = \frac{1}{2\pi}[\nabla\times\vec{K}]_{i,j,k} = n_t\sum_{i^*,j^*,k^*}\frac{\delta_{i,i^*}\delta_{j,j^*}\delta_{k,k^*}}{\Delta x^2}\vec{e}_{i^*,j^*,k^*}. \tag{11}$$

Therefore, the topological charge vector at each grid is

$$\begin{aligned}\vec{\rho}(i,j,k)\Delta x^2 &= \frac{1}{2\pi}[\nabla\times\vec{K}]_{i,j,k}\Delta x^2\\ &= n_t\sum_{i^*,j^*,k^*}\delta_{i,i^*}\delta_{j,j^*}\delta_{k,k^*}\vec{e}_{i^*,j^*,k^*}.\end{aligned} \tag{12}$$

Equation (12) contains some valuable information for us. Firstly, (i^*, j^*, k^*) represents the coordinate of the intersection of the filament and a local section Δx^2, so there must be a topological charge vector $\vec{\rho}(i,j,k)\Delta x^2$ with modulus 1 at the intersection of the filament and the local section Δx^2. It is worth noting that there are only three types of local sections with the area Δx^2 in a three-dimensional discrete space: the $\Delta x-\Delta y$ section, the $\Delta y-\Delta z$ section, and the $\Delta x-\Delta z$ section. Secondly, the topological charge vector $\vec{\rho}(i,j,k)\Delta x^2$ only points in a direction perpendicular to one of these three sections, which agrees with that given by applying the right-hand rule to the spiral wave on the local section Δx^2. In other words, the direction of $\vec{\rho}(i,j,k)\Delta x^2$ is parallel or antiparallel to the direction of the coordinate axis.

Obviously, the key to the calculations is

$$\begin{aligned}\frac{1}{2\pi}[\nabla\times\vec{K}]\Delta x^2 = \frac{1}{2\pi}\bigg[&\left(\frac{\partial^2\phi}{\partial z\partial y}-\frac{\partial^2\phi}{\partial y\partial z}\right)\vec{e}_x\\ &+\left(\frac{\partial^2\phi}{\partial x\partial z}-\frac{\partial^2\phi}{\partial z\partial x}\right)\vec{e}_y\\ &+\left(\frac{\partial^2\phi}{\partial y\partial x}-\frac{\partial^2\phi}{\partial x\partial y}\right)\vec{e}_z\bigg]\Delta x^2.\end{aligned} \tag{13}$$

As for the numerical simulation, we take the z component as an example to show the computation. Actually, a three-dimensional discrete space $\phi(i,j,k)$ can be regarded as a stack of two-dimensional layers k and each layer k is formed by grids $\phi(i,j)$. The topological charge-density method discussed in Ref. [23] is the method to calculate $\frac{1}{2\pi}(\frac{\partial^2\phi}{\partial y\partial x}-\frac{\partial^2\phi}{\partial x\partial y})\Delta x^2$ in a two-dimensional layer. For more details about the computation of the topological charge-density method with a 2×2 array and a 3×3 array, please read Appendix A. If we apply the topological charge-density method to each layer k, it will help us obtain $\frac{1}{2\pi}(\frac{\partial^2\phi}{\partial y\partial x}-\frac{\partial^2\phi}{\partial x\partial y})\Delta x^2$ at each layer k. Finally, we get the z component of Eq. (13) in a three-dimensional discrete space.

The other two components of Eq. (13) may be calculated in a similar manner. As a result, the distribution of topological charge vectors in a three-dimensional discrete space can be obtained by the calculation of Eq. (13).

The result obtained by the topological charge-density-vector method with a 2×2 array is straightforward: topological charge vectors with modulus 1 are distributed in the three-dimensional discrete space. Each topological charge vector has a corresponding local section Δx^2, as shown in Fig. 1. The starting point of the topological charge vector is located at the center of the local section Δx^2 and its direction is normal to the local section Δx^2.

The result obtained by the topological charge-density-vector method with a 3×3 array is slightly different: vectors with modulus 0.25 are distributed in the three-dimensional discrete space. From its partial, enlarged view, we found a situation similar to that in Fig. 2(a) in Ref. [23]. There are four vectors with modulus 0.25 in the same direction on the local section Δx^2 with the filament passing through. The distribution of these four vectors is similar to that of the black squares in Fig. 2(a) of Ref. [23]. Like the operation in Ref. [23], these four vectors will sum up to a topological charge vector with modulus 1, located in the center of the local section Δx^2. In this way we can get the same result as that of the topological charge-density-vector method with a 2×2 array.

B. Other methods

In the zero-normal-velocity method developed by Fenton and Karma [18], the filament is defined by the line of intersection of the two surfaces:

$$V(\vec{r},t) = V^*, \quad \partial_t V(\vec{r},t) = 0. \tag{14}$$

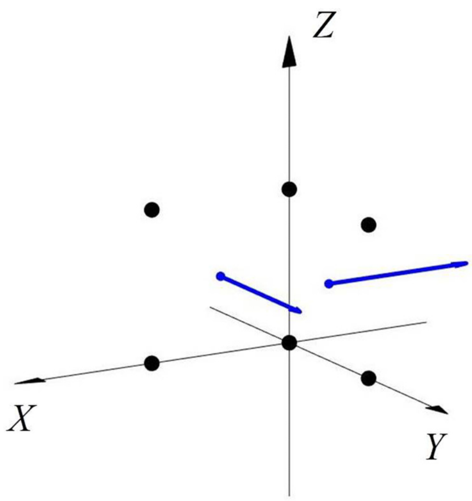

FIG. 1. The partial, enlarged view of the distribution of topological charge vectors obtained by the topological charge-density-vector method with 2×2 array. Black dots are the grids in the three-dimensional discrete space. A blue vector with modulus 1 represents a topological charge vector, which is located at the center of the local section Δx^2.

In simulations and experiments, $\partial_t V(\vec{r}, t)$ can be calculated roughly from $\partial_t V(\vec{r}, t) = [V(\vec{r}, t+\tau) - V(\vec{r}, t)]/\tau$. The task of identifying the filament is then reduced to finding the line of intersection of the two surfaces defined by

$$V(\vec{r}, t) = V(\vec{r}, t+\tau) = V^*. \tag{15}$$

Fenton and Karma represent this line by the set of intersection points of this line with the local section Δx^2. To find the points of intersection of this line with a local section Δx^2, they simply approximate $V(\vec{r}, t)$ and $V(\vec{r}, t+\tau)$ inside this section Δx^2 by a bilinear interpolation formula. There exists an intersection of the filament with this section Δx^2 if $V(\vec{r}, t) = V(\vec{r}, t+\tau) = V^*$ has a solution. Δx is divided into N_Δ equal intervals for bilinear interpolation. If there is a point that satisfies $|V(\vec{r}, t) - V^*| < V_{\rm diff}$ and $|V(\vec{r}, t+\tau) - V^*| < V_{\rm diff}$, this point is regarded as an intersection of the filament with a section Δx^2. For detail, please see the algorithm described in Ref. [18], Sec. VI, and Appendix B.

When τ is extremely small, e.g., $\tau = \Delta t \ll 1$, the calculated results are not robust for the localization of the phase singularity of a spiral wave [36]. For practical usage, the time delay τ tends to take a longer time interval rather than Δt [37,38]. Thus, we make τ in this method consistent with the one mentioned in Eq. (5), namely, $\tau = 0.1T$.

For comparison, the second method we use for the identification of a filament is the convolution method developed by Bray and Wikswo [21]. They proposed that $\nabla \times \vec{K}$ in Eq. (12) can be expressed as a convolution operation:

$$\begin{aligned}\nabla \times \vec{K} = \big[&\big(\nabla_z^x \otimes K_y + \nabla_y^x \otimes K_z\big)\vec{e}_x \\ &+ \big(\nabla_x^y \otimes K_z + \nabla_z^y \otimes K_x\big)\vec{e}_y \\ &+ \big(\nabla_x^z \otimes K_y + \nabla_y^z \otimes K_x\big)\vec{e}_z\big]/\Delta x,\end{aligned} \tag{16}$$

where $\otimes$ is the convolution operator, and

$$\begin{aligned}K_x &= [\phi(i+1, j, k) - \phi(i, j, k)]/\Delta x,\\ K_y &= [\phi(i, j+1, k) - \phi(i, j, k)]/\Delta x,\\ K_z &= [\phi(i, j, k+1) - \phi(i, j, k)]/\Delta x.\end{aligned}$$

It should be ensured that the value of the phase change between two grids is within the range $(-\pi, +\pi]$. ∇_z^x, ∇_y^x, ∇_x^y, ∇_z^y, ∇_x^z, and ∇_y^z are convolution kernels. We use the convolution method to find the filament following the operation described in Ref. [21]. That is, the convolution kernels are nabla 2×2 kernels and the filaments are delineated as the points of which the convolutional results are nonzero; the filaments are finally visualized by making the isosurface of the grids using a threshold of zero.

IV. RESULTS

In this section, we demonstrate the applicability of the topological charge-density-vector method to locate filaments in three-dimensional excitable media and compare its performance with other methods. All computer programs were coded in FORTRAN 90, and all simulations were implemented on a Sugon TC6000 computer.

The first model we chose for numerical simulation is the FHN model. We apply the topological charge-density-vector method to an arbitrary scroll wave and select a segment as the research object, whose topological charge vectors are displayed in Fig. 2(a) marked in blue. Figure 2(a) shows that the spatial distribution of the topological charge vectors can be used for the description of the filament. Figure 2(b) is the filament formed by the starting points of topological charge vectors in Fig. 2(a), but it is not smooth enough due to discretization. According to the method described in Appendix B, we process the filament and show the result in Fig. 2(c). Compared with the filament formed by the starting points directly, the processed filament no longer has obvious creases. The results shown in both Figs. 2(b) and 2(c) can be regarded as the filament. In this paper, we choose the processed filament to display. In order to make the direction of the topological charge vector change smoothly along the filament, the direction of the topological charge vector of the processed filament will be averaged by the seven vectors (itself, and three vectors before and after it).

Figure 3 illustrates a case where the shape of the filament is an oblique line. Figure 3(a) is the filament (blue line) identified by the topological charge-density-vector method. With the filament passing through, the two sections d and e have spiral waves rotating around the filament. The topological charge vectors and the spiral waves on these two sections are shown in Figs. 3(d) and 3(e), respectively. The topological charge vectors in Figs. 3(d) and 3(e) are appropriately magnified, making it easier to observe. The direction of the topological charge vector also reveals the direction in which the filament passes through a section. In other words, the spatial orientation of the filament on a section given by the topological charge vector agrees with the direction given by applying the right-hand rule to the spiral wave on that section. Figures 3(b) and 3(c) are the filaments identified by the zero-normal-velocity method (red line) and the convolution method

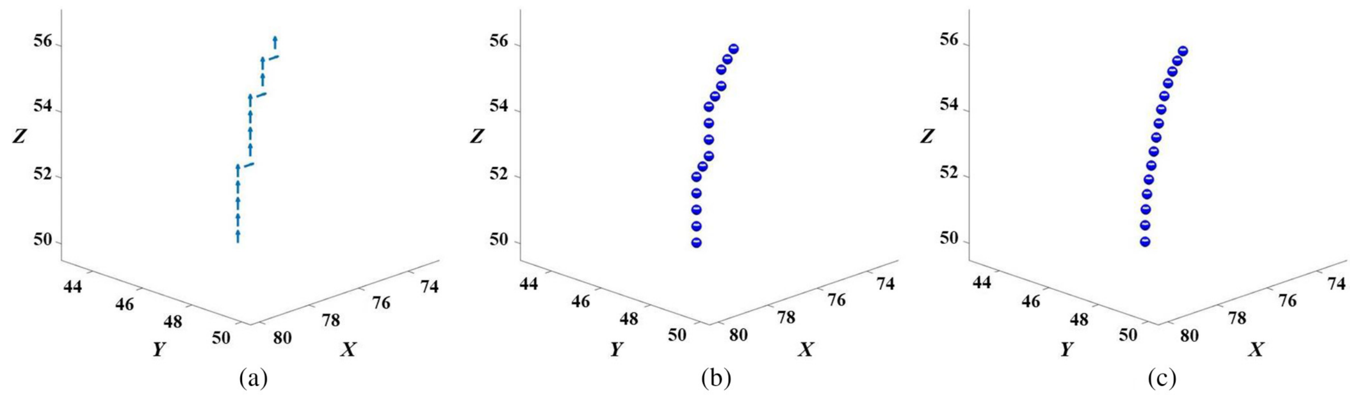

FIG. 2. (a) Topological charge vectors of a filament. The blue dots in (b), (c) represent the starting points of topological charge vectors. (b) The starting points without processing. (c) The starting points after processing.

(green line), respectively. Comparing Figs. 3(a)–3(c), the filament positions located by these three methods are basically the same.

Not only can the filament of the scroll wave end on the boundary of the space, but it also typically forms an unknotted closed ring itself. The scroll "unknot", i.e., a scroll ring, is believed to be capable of occurring in cardiac tissue [39,40]. We take it into consideration to test our method; the result is illustrated in Fig. 4(a). It is known from Figs. 4(d) and 4(e), and Figs. 4(f) and 4(g) that the chirality of spiral waves on sections d and e, and sections f and g are opposite, respectively, which reveals the fact that the direction of the topological charge vector changes continuously along the ring. The filament located by the zero-normal-velocity method is shown in Fig. 4(b), and Fig. 4(c) is the filament obtained by the convolution method. Although these three filaments have some difference in detail, their positions are roughly the same.

In a three-dimensional medium, these scroll rings may be linked and knotted in specific, allowed ways, which has aroused widespread attention over the recent years [41–44]. The simplest case for linked filaments in a three-dimensional space is two rings linked once [42], known as the Hopf link. To create the initial condition of this link, we apply the method introduced in Ref. [45]. The filament of this link identified

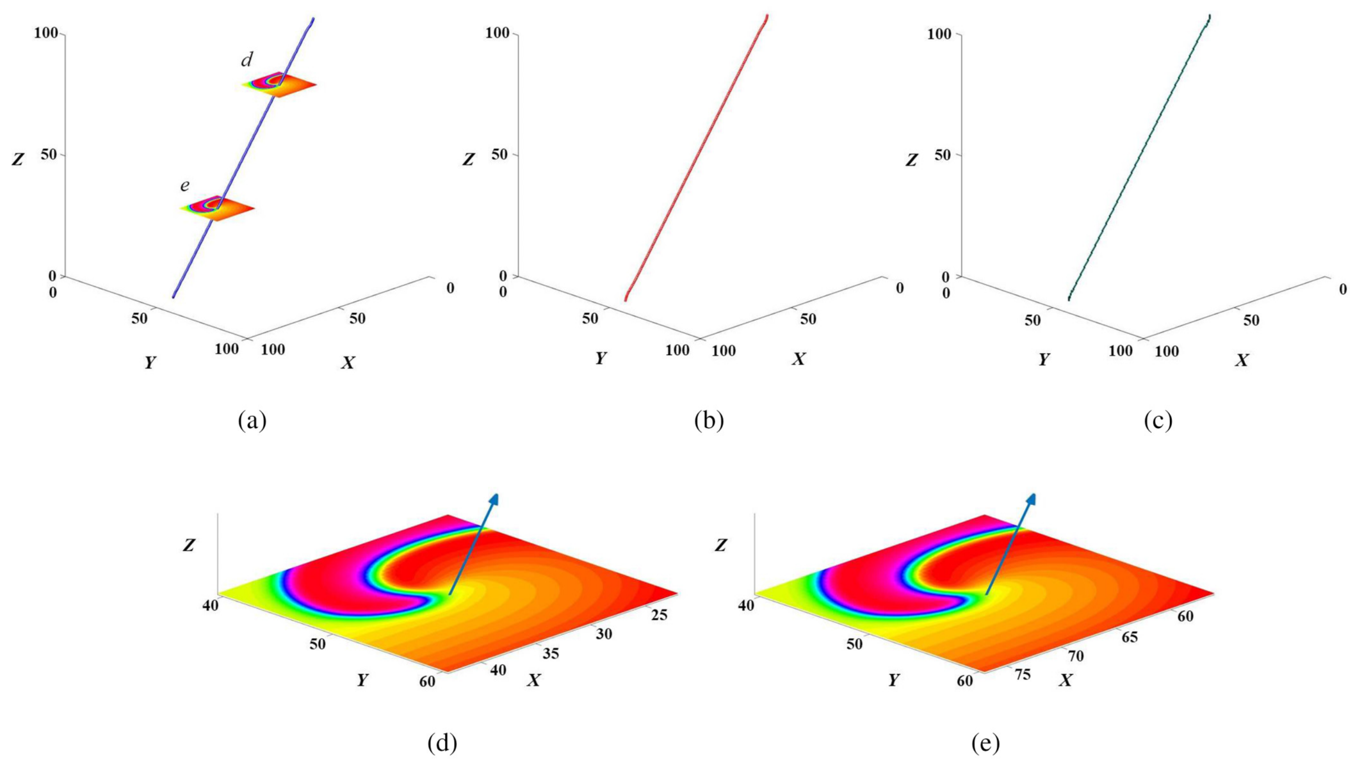

FIG. 3. (a) The filament identified by the topological charge-density-vector method. The two sections d and e have spiral waves rotating around the filament. (b) The filament identified by the zero-normal-velocity method with $N_{\Delta} = 100$ and $V_{\text{diff}} = 0.001$. (c) The filament identified by the convolution method. (d) The topological charge vector and the spiral wave on section d. (e) The topological charge vector and the spiral wave on section e.

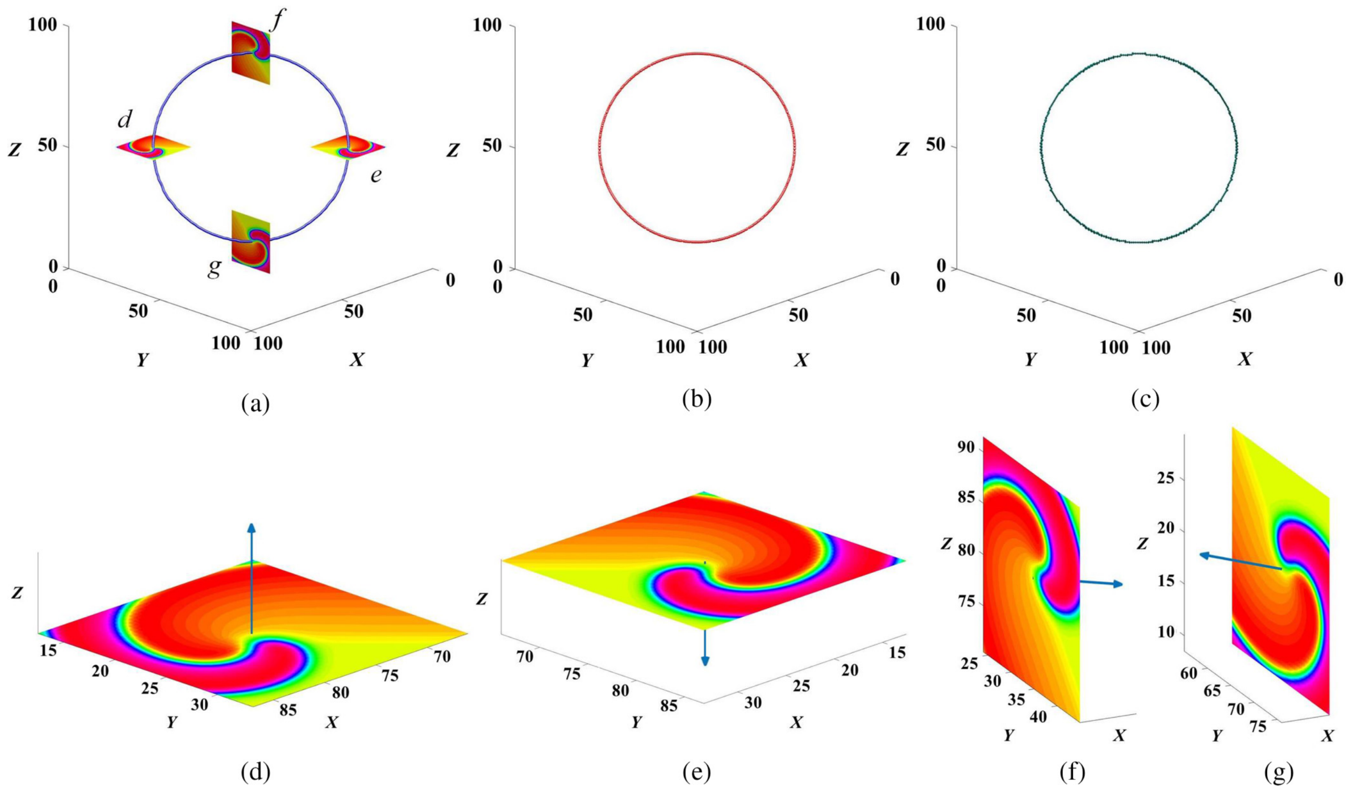

FIG. 4. (a) The filament identified by the topological charge-density-vector method. The four sections d, e, f, and g have spiral waves rotating around the filament. (b) The filament identified by the zero-normal-velocity method with $N_\Delta = 100$ and $V_{\mathrm{diff}} = 0.001$. (c) The filament identified by the convolution method. (d) The topological charge vector and the spiral wave on section d. (e) The topological charge vector and the spiral wave on section e. (f) The topological charge vector and the spiral wave on section f. (g) The topological charge vector and the spiral wave on section g.

by the topological charge-density-vector method is presented in Fig. 5(a). We mark some topological charge vectors of this linked filament at some positions in Fig. 5(a), and they give the direction of the filament at those positions. For comparison, we show the filaments obtained by the other two methods in Figs. 5(b) and 5(c), respectively.

The simplest nontrivial knot is the trefoil knot, whose structure is well displayed in Ref. [46]. To create the initial condition of the trefoil knot, we use the method introduced in Ref. [47]. After waiting for the scroll wave to run stably, we use these three methods to identify the filament and the results are shown in Figs. 5(d)–5(f). We also mark some topological charge vectors of this knotted filament in Fig. 5(d). Unlike the filaments in Figs. 5(d) and 5(f), we find that the filament in Fig. 5(e) identified by the zero-normal-velocity method is discontinuous.

Obtained by the topological charge-density-vector method, the topological charge vectors in Figs. 5(a) and 5(d) can reveal the direction of the filament at those positions while the other two methods may not give such information.

Meanwhile, we introduce the filament-detecting accuracy rate to judge whether a method is good enough. At first, we need to define three types of points for a filament: the accurate point, the false point, and the discontinuous point. Each time the filament passes through a local section, it leaves only one point at the local section, so if there is a point in a local section Δx^2 and no other points in the eight local sections Δx^2 around this section Δx^2, this point is defined as an accurate point. Conversely, if there are other points in the eight local sections Δx^2 around this section Δx^2, this point is defined as a false point. A discontinuous point is a point of a filament whose distance from the next point is more than $\sqrt{3}\Delta x$ (the longest distance in a cube with a side length Δx). This is because filaments should be continuous in space, which occurs on a set of one-dimensional curves that may be either closed loops or infinite curves [48–50]. The appearance of the discontinuous point and the false point will make the total accurate point number of a filament found by a method be less than the total point number of the "true filament". The filament-detecting accuracy rate is defined as the total accurate point number of a filament found by a method divided by the total point number of the "true filament".

With different τ and different spatial resolution, we calculated the filament-detecting accuracy rates of the topological charge-density-vector method and the zero-normal-velocity method in the cases of Fig. 5. In all the cases shown in Tables I and II, we find that the filaments identified by the topological charge-density-vector method have neither a false point nor a discontinuous point. Therefore, we regard the filament identified by the topological charge-density-vector method as the "true filament". Namely, the filament-detecting accuracy rate is 100%. Then, the filament-detecting accuracy rate of the zero-normal-velocity method is the total accurate point number of the filament found by the zero-normal-velocity method

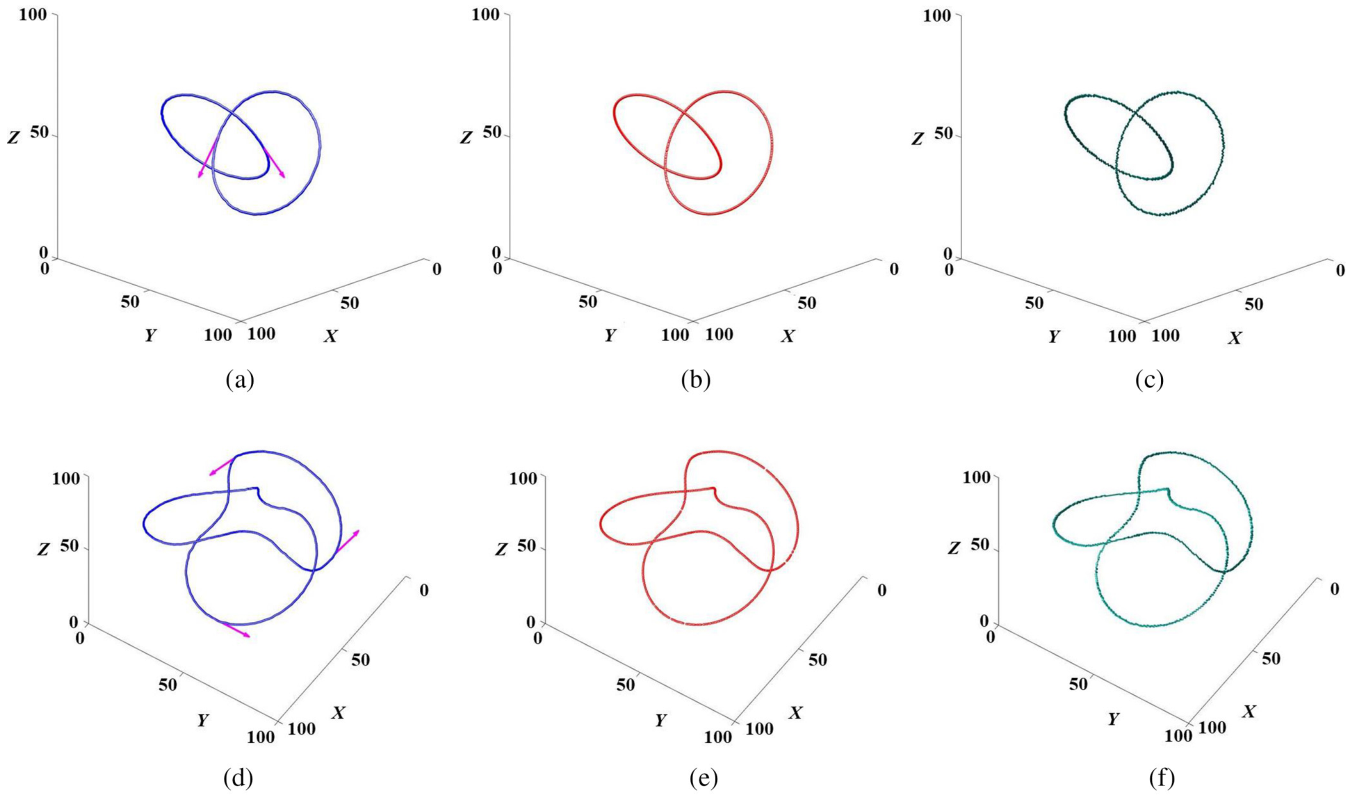

FIG. 5. (a) The filament of the Hopf link identified by the topological charge-density-vector method. The arrows in (a) represent the topological charge vectors. (b) The filament of the Hopf link identified by the zero-normal-velocity method with $N_\Delta = 100$ and $V_{\text{diff}} = 0.001$. (c) The filament of the Hopf link identified by the convolution method. (d) The filament of the trefoil knot identified by the topological charge-density-vector method. The arrows in (d) represent the topological charge vectors. (e) The filament of the trefoil knot identified by the zero-normal-velocity method with $N_\Delta = 100$ and $V_{\text{diff}} = 0.001$. (f) The filament of the trefoil knot identified by the convolution method.

divided by the total accurate point number of the filament found by the topological charge-density-vector method, which is given in the last column of the table. We list the filament-detecting accuracy rate of the zero-normal-velocity method with $N_\Delta = 100$, $V_{\text{diff}} = 0.001$ and $N_\Delta = 100$, $V_{\text{diff}} = 0.002$ in the table. N_Δ controls the number of interpolation in Δx^2, which greatly affects the computational time and interpolation results. V_{diff} controls the number of the discontinuous point and the false point: a smaller V_{diff} will cause more discontinuous points, while a larger V_{diff} will cause more false points. Setting N_Δ and V_{diff} in this way may obtain acceptable results with an appropriate computational time. The convolution method is not included in statistics because its filaments are visualized by making the zero-threshold

TABLE I. The filament-detecting accuracy rate of the zero-normal-velocity method with different τ. The data under the headings “Zero-normal-velocity method” and “Topological charge-density-vector method” are in the form of “total accurate point number/total number (computational time).” “Accuracy rate” is the result of the total accurate point number of the filament found by the zero-normal-velocity method divided by the total accurate point number of the filament found by the topological charge-density-vector method.

	τ	Zero-normal-velocity method			Topological charge-density-vector method	Accuracy rate
Link	$0.05T$	$N_\Delta = 100$	$V_{\text{diff}} = 0.001$	861/987 (0.139 s)	924/924 (0.760 s)	93.18%
		$N_\Delta = 100$	$V_{\text{diff}} = 0.002$	757/1101 (0.139 s)		81.93%
	$0.10T$	$N_\Delta = 100$	$V_{\text{diff}} = 0.001$	837/1001 (0.136 s)	928/928 (0.534 s)	90.19%
		$N_\Delta = 100$	$V_{\text{diff}} = 0.002$	761/1097 (0.137 s)		82.00%
	$0.20T$	$N_\Delta = 100$	$V_{\text{diff}} = 0.001$	864/938 (0.147 s)	932/932 (0.522 s)	92.70%
		$N_\Delta = 100$	$V_{\text{diff}} = 0.002$	838/1030 (0.138 s)		89.91%
Knot	$0.05T$	$N_\Delta = 100$	$V_{\text{diff}} = 0.001$	1411/1566 (0.349 s)	1522/1522 (0.775 s)	92.71%
		$N_\Delta = 100$	$V_{\text{diff}} = 0.002$	1319/1748 (0.353 s)		86.66%
	$0.10T$	$N_\Delta = 100$	$V_{\text{diff}} = 0.001$	1333/1377 (0.217 s)	1524/1524 (0.529 s)	87.47%
		$N_\Delta = 100$	$V_{\text{diff}} = 0.002$	1436/1618 (0.220 s)		94.23%
	$0.20T$	$N_\Delta = 100$	$V_{\text{diff}} = 0.001$	1124/1136 (0.161 s)	1528/1528 (0.528 s)	73.56%
		$N_\Delta = 100$	$V_{\text{diff}} = 0.002$	1486/1557 (0.163 s)		97.25%

TABLE II. The filament-detecting accuracy rate of the zero-normal-velocity method with different spatial resolution.

	Spatial resolution	Zero-normal-velocity method			Topological charge-density-vector method	Accuracy rate
Link	$100 \times 100 \times 100$	$N_\Delta = 100$	$V_{\text{diff}} = 0.001$	378/390 (0.038 s)	460/460 (0.092 s)	82.17%
		$N_\Delta = 100$	$V_{\text{diff}} = 0.002$	430/462 (0.040 s)		93.48%
	$50 \times 50 \times 50$	$N_\Delta = 100$	$V_{\text{diff}} = 0.001$	108/108 (0.016 s)	228/228 (0.012 s)	47.37%
		$N_\Delta = 100$	$V_{\text{diff}} = 0.002$	174/174 (0.034 s)		76.32%
Knot	$100 \times 100 \times 100$	$N_\Delta = 100$	$V_{\text{diff}} = 0.001$	302/308 (0.081 s)	762/762 (0.094 s)	39.63%
		$N_\Delta = 100$	$V_{\text{diff}} = 0.002$	615/631 (0.082 s)		80.71%
	$50 \times 50 \times 50$	$N_\Delta = 100$	$V_{\text{diff}} = 0.001$	49/49 (0.065 s)	379/379 (0.013 s)	12.93%
		$N_\Delta = 100$	$V_{\text{diff}} = 0.002$	147/153 (0.067 s)		38.79%

isosurface of the grids where the convolutional results are nonzero.

Table I shows the filament-detecting accuracy rate of the zero-normal-velocity method with different τ. By uniformly spaced sampling of the original system, $200 \times 200 \times 200$, Table II shows the filament-detecting accuracy rate of the zero-normal-velocity method in low spatial resolutions: the spatial step is changed from Δx to $2\Delta x$ for $100 \times 100 \times 100$ and is changed from Δx to $4\Delta x$ for $50 \times 50 \times 50$. Table II illustrates that the performance of the zero-normal-velocity method in low spatial resolution is not very good, especially in the case of the knotted filament.

Figure 6 is a system in a completely disorganized state simulated by the Bär model. We use the topological charge-density-vector method to detect the complex filaments of scroll wave turbulence and the result is illustrated in Fig. 6(a) with computational time 0.105 s. Not only is our method effective in detecting the complex and chaotic filaments, but it also can point out the direction of the filaments, as the topological charge vectors shown in Fig. 6(a). The result of the zero-normal-velocity method is presented in Fig. 6(b) and the computational time is 0.172 s. We find the filaments in Fig. 6(b) are discontinued at some positions with careful observation. Taking 0.490 s for Fig. 6(c), the filaments identified by the convolution method are basically consistent with those in Fig. 6(a), while, unlike the topological charge-density-vector method shown in Fig. 6(a), the zero-normal-velocity method and the convolution method may not give the direction of the filament.

We further calculated the filament-detecting accuracy rate of the topological charge-density-vector method and the zero-normal-velocity method in Figs. 6(a) and 6(b), respectively. All filaments identified by the topological charge-density-vector method are continuous without false points. So we regard those filaments as the "true filaments" and the filament-detecting accuracy rate of the topological charge-density-vector method is 100%. The filament-detecting accuracy rate of the zero-normal-velocity method is shown in Table III.

Now we investigate whether the topological charge-density-vector method is also applicable to the cardiac model. The scroll wave turbulence in Fig. 7 is generated by the Luo-Rudy model. In Fig. 7(a), we plot topological charge vectors of the scroll wave calculated by the topological charge-density-vector method. Figure 7(b) shows the starting points of topological charge vectors after processing. When using the zero-normal-velocity method to identify the filament in the Luo-Rudy model, we set $N_\Delta = 100$ and $V_{\text{diff}} = 0.1$ mV. The filament identified by the zero-normal-velocity method is shown in Fig. 7(c). We can see that the filaments in Fig. 7(c) are discontinued at some positions. Figure 7(d) is the result obtained by the convolution method. From the results shown in Fig. 7, we know that the performance of the topological charge-density-vector method in the Luo-Rudy model is satisfactory.

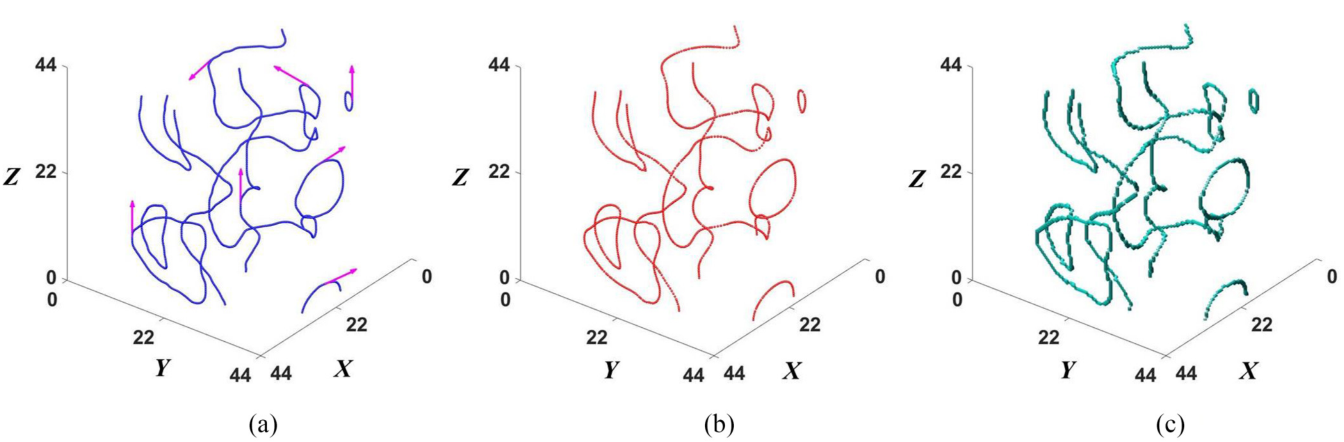

FIG. 6. The complex filaments of scroll wave turbulence simulated by the Bär model. (a) The filaments identified by the topological charge-density-vector method. The arrows in (a) represent the topological charge vectors. (b) The filaments identified by the zero-normal-velocity method with $N_\Delta = 100$ and $V_{\text{diff}} = 0.001$. (c) The filaments identified by the convolution method.

TABLE III. The filament-detecting accuracy rate of the zero-normal-velocity method in the Bär model.

Zero-normal-velocity method			Topological charge-density-vector method	Accuracy rate
$N_{\Delta} = 100$	$V_{\text{diff}} = 0.001$	1374/1804 (0.172 s)	1561/1561 (0.105 s)	88.02%
$N_{\Delta} = 100$	$V_{\text{diff}} = 0.002$	1141/2099 (0.176 s)		73.09%

V. DISCUSSION

From the previous discussions and comparisons, we conclude that the topological charge-density-vector method has the following three advantages. First, compared with the convolution method, the topological charge-density-vector method is strictly derived in theory and the algorithm used in numerical simulations is unique and simple. Second, compared with the zero-normal-velocity method, the topological charge-density-vector method is more robust in the cases of this paper. The performance of the zero-normal-velocity method is unstable and affected by N_{Δ} and V_{diff}. Third, the topological charge vector obtained by our method reveals the direction of the filament passing through a local section Δx^2, which agrees with the direction given by applying the right-hand rule to the spiral wave on that section.

The direct extension of the two-dimensional topological charge-density method [23] into three dimensions can indeed be used to find the filament: a three-dimensional discrete space can be regarded as a stack of two-dimensional planes xy along the z axis; the phase singularities in each plane are identified by the two-dimensional topological charge-density method; one can get the filament by connecting these phase singularities. However, such calculations fail to identify the parts of the filaments parallel to the xy plane. This is why we need the topological charge-density-vector method, which is a complete theory derived from the concept of topological charge in three-dimensional space.

Our method requires choosing the state space origin V^*. Gray *et al.* [29] pointed out that the choice of V^* influences the identification of the phase singularity in two dimensions. For example, inappropriate origin choice will lead to an error in the identification of the number and the lifetime of spiral waves. The best choice of V^* can be obtained for simple models such as FHN; however, in realistic cardiac myocyte models and in experiments, V^* is hard to obtain [29].

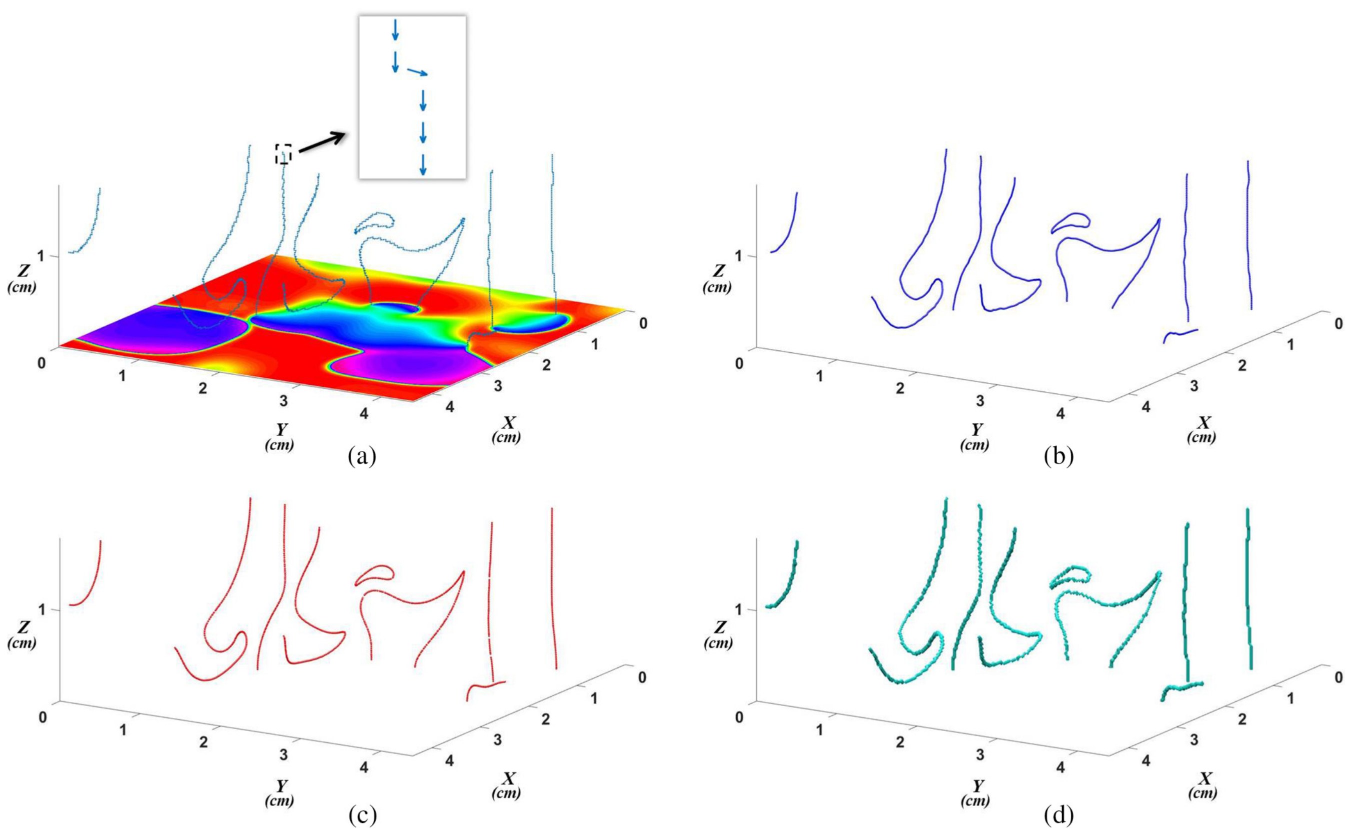

FIG. 7. Filaments of scroll wave turbulence simulated by the Luo-Rudy model. (a) Topological charge vectors of the filament calculated by the topological charge-density-vector method. The inset shows the details of vector distributions. (b) The starting points of topological charge vectors after processing. (c) The filament identified by the zero-normal-velocity method with $N_{\Delta} = 100$ and $V_{\text{diff}} = 0.1$ mV. (d) The filament identified by the convolution method.

The PEMD [33] is a reliable method for phase calculation without the choice of V^*. The first step of PEMD is to construct the envelope of the maximum and the minimum of $V(t)$, marked $V_{\max}(t)$ and $V_{\min}(t)$, respectively. Then we get the envelope midline $V_{\text{mean}}(t)$ by

$$V_{\text{mean}}(x, y, z, t) = \frac{V_{\max}(x, y, z, t) + V_{\min}(x, y, z, t)}{2}.$$

Making a similar operation on $V(t+\tau)$, we obtain

$$V_{\text{mean}}(x, y, z, t+\tau) = \frac{V_{\max}(x, y, z, t+\tau) + V_{\min}(x, y, z, t+\tau)}{2}.$$

Finally, the expression of the phase is

$$\phi(x, y, z, t) = \arctan 2[V(x, y, z, t+\tau) - V_{\text{mean}}(x, y, z, t+\tau), V(x, y, z, t) - V_{\text{mean}}(x, y, z, t)].$$

At present, the main problem with using PEMD is that this method is too time consuming in a three-dimensional case to be used in our work. However, through parallel computing, the problem may be solved.

VI. CONCLUSION

In summary, we have developed a method for detecting filaments of scroll waves, named the topological charge-density-vector method. The discrete expression of the topological charge-density vector of the filament is derived from the topological current theory and the concept of topological charge. According to this discrete expression, we calculate the topological charge vector at each grid in the three-dimensional space directly, which is useful for the description of the filament. Topological charge vectors are vectors with modulus 1 at the positions of the filament, with modulus 0 at other positions, and the direction of the topological charge vector agrees with the direction given by applying the right-hand rule to the spiral wave on that section. By connecting the starting points of the topological charge vectors directly or operating these starting points properly, we can locate the position of the filament. In the three-dimensional excitable medium simulated by the FHN model, we illustrate the effectiveness of this method with the scroll waves of specific shapes, including the linked and knotted filaments. For the complex filaments of scroll wave turbulence simulated by the Bär model, the topological charge-density-vector method shows the robustness of the filament identification. We further apply this method to the scroll wave turbulence in the Luo-Rudy model, and the result is satisfactory.

Having strictly theoretical derivation, the topological charge-density-vector method is available for research of the filament localization. The numerical simulation results suggest that the algorithm of this method is practical and robust. We therefore expect that the topological charge-density-vector method will make a positive contribution towards exploring the general theory of scroll waves and the mechanism of ventricular fibrillation induced by scroll waves in the future.

ACKNOWLEDGMENTS

We are grateful to A. V. Panfilov, X. Liu, X. Gao, and T.-C. Li for valuable discussions and comments. This work was supported by the National Natural Science Foundation of China under Grants No. 12075203 and No. 12175193.

APPENDIX A

Here we will show in detail how to use the topological charge-density method for numerical simulations.

The calculation described in Ref. [23] involves a lot of finite difference operations. Thus, the key point of the algorithm is to realize the operation $\phi(i+1, j) - \phi(i, j)$ efficiently. When designing the algorithm, only one calculation is needed to obtain $\phi(i+1, j) - \phi(i, j)$ at each grid with the array $\phi(2 : N_x, 1 : N_y)$ minus the array $\phi(1 : N_x{-}1, 1 : N_y)$ directly. The operation in the y direction also uses one calculation. This algorithm greatly simplifies the calculation. Based on this algorithm, the topological charge-density method is performed as follows.

1. Topological charge-density method with 3 × 3 array

The gradient of the phase at each grid is defined as

$$\frac{\partial \phi}{\partial x}(i, j) = \frac{1}{2}\left[\frac{\phi(i+1, j) - \phi(i, j)}{\Delta x} + \frac{\phi(i, j) - \phi(i-1, j)}{\Delta x}\right], \tag{A1a}$$

$$\frac{\partial \phi}{\partial y}(i, j) = \frac{1}{2}\left[\frac{\phi(i, j+1) - \phi(i, j)}{\Delta x} + \frac{\phi(i, j) - \phi(i, j-1)}{\Delta x}\right]. \tag{A1b}$$

All terms on the right side of Eqs. (A1a) and (A1b) can be solved by the above algorithm. It should be ensured that the value of the phase change between two grids is within the range $(-\pi, +\pi]$.

Using a similar operation, namely, with the array $\frac{\partial \phi}{\partial x}(1 : N_x, 3 : N_y)$ minus the array $\frac{\partial \phi}{\partial x}(1 : N_x, 1 : N_y{-}2)$ and with the array $\frac{\partial \phi}{\partial y}(3 : N_x, 1 : N_y)$ minus the array $\frac{\partial \phi}{\partial y}(1 : N_x{-}2, 1 : N_y)$ directly, we get

$$\frac{\partial^2 \phi}{\partial x \partial y}(i, j) = \frac{\frac{\partial \phi}{\partial x}(i, j+1) - \frac{\partial \phi}{\partial x}(i, j-1)}{2\Delta x}, \tag{A2a}$$

$$\frac{\partial^2 \phi}{\partial y \partial x}(i, j) = \frac{\frac{\partial \phi}{\partial y}(i+1, j) - \frac{\partial \phi}{\partial y}(i-1, j)}{2\Delta x}, \tag{A2b}$$

at each grid. Finally, we have $\rho(i, j)\Delta x^2$ by

$$\frac{1}{2\pi}\left[\frac{\partial^2 \phi}{\partial y \partial x}(i, j) - \frac{\partial^2 \phi}{\partial x \partial y}(i, j)\right]\Delta x^2. \tag{A3}$$

2. Topological charge-density method with 2 × 2 array

The gradient of the phase at each grid is defined as

$$\frac{\partial \phi}{\partial x}\left(i+\frac{1}{2}, j\right)=\frac{\phi(i+1, j)-\phi(i, j)}{\Delta x}, \tag{A4a}$$

$$\frac{\partial \phi}{\partial y}\left(i, j+\frac{1}{2}\right)=\frac{\phi(i, j+1)-\phi(i, j)}{\Delta x}, \tag{A4b}$$

which is easily calculated by the above algorithm.

With the array $\frac{\partial\phi}{\partial x}(1+\frac{1}{2}:N_x-\frac{1}{2}, 2:N_y)$ minus the array $\frac{\partial\phi}{\partial x}(1+\frac{1}{2}:N_x-\frac{1}{2}, 1:N_y-1)$ and with the array $\frac{\partial\phi}{\partial y}(2:N_x, 1+\frac{1}{2}:N_y-\frac{1}{2})$ minus the array $\frac{\partial\phi}{\partial y}(1:N_x-1, 1+\frac{1}{2}:N_y-\frac{1}{2})$ directly, we have

$$\frac{\partial^2 \phi}{\partial x \partial y}\left(i+\frac{1}{2}, j+\frac{1}{2}\right)=\frac{\frac{\partial \phi}{\partial x}\left(i+\frac{1}{2}, j+1\right)-\frac{\partial \phi}{\partial x}\left(i+\frac{1}{2}, j\right)}{\Delta x}, \tag{A5a}$$

$$\frac{\partial^2 \phi}{\partial y \partial x}\left(i+\frac{1}{2}, j+\frac{1}{2}\right)=\frac{\frac{\partial \phi}{\partial y}\left(i+1, j+\frac{1}{2}\right)-\frac{\partial \phi}{\partial y}\left(i, j+\frac{1}{2}\right)}{\Delta x}, \tag{A5b}$$

at each grid. As a result, we have $\rho(i+\frac{1}{2}, j+\frac{1}{2})\Delta x^2$ by

$$\frac{1}{2\pi}\left[\frac{\partial^2 \phi}{\partial y \partial x}\left(i+\frac{1}{2}, j+\frac{1}{2}\right)-\frac{\partial^2 \phi}{\partial x \partial y}\left(i+\frac{1}{2}, j+\frac{1}{2}\right)\right]\Delta x^2. \tag{A6}$$

APPENDIX B

Figure 8(a) is a set of starting points of topological charge vectors without processing. The initial coordinate $\vec{S}(m)$ at each point is $[S_x(m), S_y(m), S_z(m)]$. Figure 8(b) is a set of starting points of topological charge vectors after processing, whose coordinate $\vec{S}'(m)$ at each point is $[S'_x(m), S'_y(m), S'_z(m)]$. $\vec{S}'(m)$ is the weighed sum of the coordinates and it is calculated by

$$\begin{aligned}
S'_x(m) = {} & q_1 \times S_x(m-3) + q_2 \times S_x(m-2) + q_3 S_x(m-1) \\
& + q_4 \times S_x(m) + q_5 \times S_x(m+1) \\
& + q_6 \times S_x(m+2) + q_7 \times S_x(m+3), \\
S'_y(m) = {} & q_1 \times S_y(m-3) + q_2 \times S_y(m-2) + q_3 S_y(m-1) \\
& + q_4 \times S_y(m) + q_5 \times S_y(m+1) \\
& + q_6 S_y(m+2) + q_7 \times S_y(m+3), \\
S'_z(m) = {} & q_1 \times S_z(m-3) + q_2 \times S_z(m-2) + q_3 S_z(m-1) \\
& + q_4 \times S_z(m) + q_5 \times S_z(m+1) \\
& + q_6 \times S_z(m+2) + q_7 \times S_z(m+3),
\end{aligned}$$

where q_α represents the weights and we set $q_1 = 0.1$, $q_2 = 0.1$, $q_3 = 0.2$, $q_4 = 0.2$, $q_5 = 0.2$, $q_6 = 0.1$, and $q_7 = 0.1$.

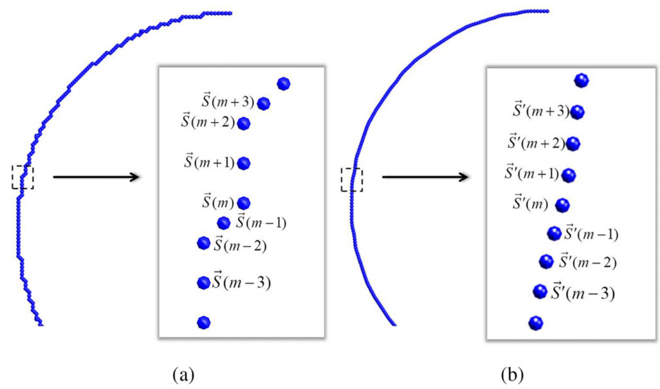

FIG. 8. (a) A set of starting points of topological charge vectors without processing and its partial, enlarged view. (b) A set of starting points of topological charge vectors after processing and its partial, enlarged view.

[1] A. T. Winfree, *When Time Breaks Down* (Princeton University Press, Princeton, NJ, 1987).
[2] V. S. Zykov, *Modelling of Wave Processes in Excitable Media* (Manchester University Press, Manchester, UK, 1988).
[3] M. C. Cross and P. C. Hohenberg, Rev. Mod. Phys. **65**, 851 (1993).
[4] A. T. Winfree, *The Geometry of Biological Time* (Springer, Berlin, 2000).
[5] K. Tsuji and S. C. Müller, *Spirals and Vortices* (Springer Nature, Cham, Switzerland, 2019).
[6] A. T. Winfree, Science **266**, 1003 (1994).
[7] R. A. Gray, J. Jalife, A. V. Panfilov, W. T. Baxter, C. Cabo, J. M. Davidenko, and A. M. Pertsov, Science **270**, 1222 (1995).
[8] A. M. Pertsov and J. Jalife, in *Cardiac Electrophysiology. From Cell to Bedside*, 2nd ed., edited by D. P. Zipes and J. Jalife (Saunders, Philadelphia, 1995), pp. 403–410.
[9] D. E. Krummen, J. Hayase, D. J. Morris, J. Ho, M. R. Smetak, P. Clopton, W.-J. Rappel, and S. M. Narayan, J. Am. Coll. Cardiol. **63**, 2712 (2014).
[10] A. T. Winfree, Science **181**, 937 (1973).
[11] A. V. Panfilov and A. N. Rudenko, Physica D (Amsterdam) **28**, 215 (1987).
[12] J. P. Keener, Physica D (Amsterdam) **31**, 269 (1988).
[13] V. N. Biktashev, A. V. Holden, and H. Zhang, Philos. Trans. R. Soc. London Ser. A **347**, 611 (1994).
[14] H. Zhang, Z. Cao, N.-J. Wu, H.-P. Ying, and G. Hu, Phys. Rev. Lett. **94**, 188301 (2005).
[15] R. H. Clayton, E. A. Zhuchkova, and A. V. Panfilov, Prog. Biophys. Mol. Biol. **90**, 378 (2006).
[16] A. Pertsov, M. Vinson, and S. C. Müller, Physica D (Amsterdam) **63**, 233 (1993).
[17] S. Mironov, M. Vinson, S. Mulvey, and A. Pertsov, J. Phys. Chem. **100**, 1975 (1996).

[18] F. Fenton and A. Karma, Chaos **8**, 20 (1998).
[19] R. A. Gray, A. M. Pertsov, and J. Jalife, Nature (London) **392**, 75 (1998).
[20] A. N. Iyer and R. A. Gray, Ann. Biomed. Eng. **29**, 47 (2001).
[21] M.-A. Bray and J. P. Wikswo, IEEE Trans. Biomed. Eng. **49**, 1086 (2002).
[22] M.-A. Bray, S.-F. Lin, R. R. Aliev, B. J. Roth, and J. P. Wikswo, Jr., J. Cardiovasc. Electrophysiol. **12**, 716 (2001).
[23] Y.-J. He, Q.-H. Li, K. Zhou, R. Jiang, C. Jiang, J.-T. Pan, D. Zheng, B. Zheng, and H. Zhang, Phys. Rev. E **104**, 014213 (2021).
[24] R. A. Gray, J. Jalife, A. Panfilov, W. T. Baxter, C. Cabo, J. M. Davidenko, and A. M. Pertsov, Circulation **91**, 2454 (1995).
[25] I. R. Efimov, V. Sidorov, Y. Cheng, and B. Wollenzier, J. Cardiovasc. Electrophysiol. **10**, 1452 (1999).
[26] A. V. Zaitsev, O. Berenfeld, S. F. Mironov, J. Jalife, and A. M. Pertsov, Circ. Res. **86**, 408 (2000).
[27] R. FitzHugh, Biophys. J. **1**, 445 (1961).
[28] J. Nagumo, S. Arimoto, and S. Yoshizawa, Proc. IRE **50**, 2061 (1962).
[29] R. A. Gray, J. P. Wikswo, and N. F. Otani, Chaos **19**, 033118 (2009).
[30] M. Bär and M. Eiswirth, Phys. Rev. E **48**, R1635(R) (1993).
[31] C. H. Luo and Y. Rudy, Circ. Res. **68**, 1501 (1991).
[32] Z. Qu, F. Xie, A. Garfinkel, and J. N. Weiss, Ann. Biomed. Eng. **28**, 755 (2000).
[33] M.-A. Bray and J. P. Wikswo, Phys. Rev. E **65**, 051902 (2002).
[34] Y. S. Duan and M. L. Ge, Sci. Sin. **11**, 1072 (1979).
[35] Y. S. Duan and H. Zhang, Phys. Rev. E **60**, 2568 (1999).
[36] T.-C. Li, D.-B. Pan, K. Zhou, R. Jiang, C. Jiang, B. Zheng, and H. Zhang, Phys. Rev. E **98**, 062405 (2018).
[37] Z. Qu, J. Kil, F. Xie, A. Garfinkel, and J. N. Weiss, Biophys. J. **78**, 2761 (2000).
[38] S. F. Pravdin, T. I. Epanchintsev, H. Dierckx, and A. V. Panfilov, Phys. Rev. E **104**, 034408 (2021).
[39] R. R. Aliev and A. V. Panfilov, J. Theor. Biol. **181**, 33 (1996).
[40] S. Alonso and A. V. Panfilov, Phys. Rev. Lett. **100**, 218101 (2008).
[41] C. Henze and A. T. Winfree, Int. J. Bifurcation Chaos **1**, 891 (1991).
[42] P. M. Sutcliffe and A. T. Winfree, Phys. Rev. E **68**, 016218 (2003).
[43] H. W. Lau and J. Davidsen, Phys. Rev. E **94**, 010204(R) (2016).
[44] J. Binysh, C. A. Whitfield, and G. P. Alexander, Phys. Rev. E **99**, 012211 (2019).
[45] F. Maucher and P. M. Sutcliffe, Nonlinearity **32**, 942 (2019).
[46] A. T. Winfree and S. H. Strogatz, Physica D (Amsterdam) **9**, 333 (1983).
[47] F. Maucher and P. M. Sutcliffe, Phys. Rev. E **96**, 012218 (2017).
[48] A. T. Winfree and S. H. Strogatz, Physica D (Amsterdam) **8**, 35 (1983).
[49] A. M. Pertsov, M. Wellner, M. Vinson, and J. Jalife, Phys. Rev. Lett. **84**, 2738 (2000).
[50] H. Zhang, B. Hu, B.-W. Li, and Y.-S. Duan, Chin. Phys. Lett. **24**, 1618 (2007).